### Title
Synthesis of surface bound silver nanoparticles on cellulose fibers using lignin as multi-functional agent




### Authors
Hu, Sixiao
Hsieh, You-Lo



### Publication Date
2015-10-01

### DOI
10.1016/j.carbpol.2015.05.060

Peer reviewed

Carbohydrate Polymers 131 (2015) 134–141

Contents lists available at ScienceDirect

Carbohydrate Polymers

journal homepage: www.elsevier.com/locate/carbpol

# Synthesis of surface bound silver nanoparticles on cellulose fibers using lignin as multi-functional agent

Sixiao Hu, You-Lo Hsieh*

*Fiber and Polymer Science, University of California-Davis, One Shields Avenue, Davis, CA 95616, United States*

ARTICLE INFO

*Article history:*
Received 15 April 2015
Received in revised form 12 May 2015
Accepted 13 May 2015
Available online 4 June 2015

*Keywords:*
Silver nanoparticle synthesis
Lignin
Cellulose nanofibers
UV absorbing
Antimicrobial

ABSTRACT

Lignin has proven to be highly effective "green" multi-functional binding, complexing and reducing agents for silver cations as well as capping agents for the synthesis of silver nanoparticles on ultra-fine cellulose fibrous membranes. Silver nanoparticles could be synthesized in 10 min to be densely distributed and stably bound on the cellulose fiber surfaces at up to 2.9% in mass. Silver nanoparticle increased in sizes from 5 to 100 nm and became more polydispersed in size distribution on larger fibers and with longer synthesis time. These cellulose fiber bound silver nanoparticles did not agglomerate under elevated temperatures and showed improved thermal stability. The presence of alkali lignin conferred moderate UV absorbing ability in both UV-B and UV-C regions whereas the bound silver nanoparticles exhibited excellent antibacterial activities toward *Escherichia coli*.



## 1. Introduction

Silver nanoparticles (AgNPs) are known to exhibit a wide spectrum of anti-microbial activities while showing low cytotoxicity and genotoxicity to human cells for biomedical applications as wound dressings, tissue scaffolds, disinfectants, surgical masks and catheters (AshaRani, Mun, Hande, & Valiyaveettil, 2009; Kim et al., 2007; Li, Leung, Yao, Song, & Newton, 2006; Maneerung, Tokura, & Rujiravanit, 2008). Typical preparation of AgNPs has involved "bottom-up" methods of reducing silver cations then stabilizing with capping reagents to various shapes and sizes from 2 to 200 nm in solutions (Sun & Xia, 2002a,b; Yamamoto, Kashiwagi, & Nakamoto, 2006). The potential toxicity of isolated silver nanoparticles in contact with human cells have raised serious concerns (Batchelor-McAuley, Tschulik, Neumann, Laborda, & Compton, 2014; Gliga, Skoglund, Wallinder, Fadeel, & Karlsson, 2014) that immobilization of silver nanoparticles have been approached for safer applications. Meanwhile, smaller AgNPs (9.2 vs 62 nm) have shown higher anti-microbial activities on equivalent mass basis (Lok et al., 2007), reducing their tendency to aggregate or coalesce have been achieved by immobilizing AgNPs on various solids such as stainless steel (Jiang, Manolache, Wong, & Denes, 2004), reverse osmosis membrane (Ben-Sasson et al., 2014), silicone (Jiang et al., 2004), glass (Taglietti et al., 2014), poly(acrylic acid) and poly(allylamine hydrochloride) films (Wang, Rubner, & Cohen, 2002), cotton fabric (El-Shishtawy, Asiri, Abdelwahed, & Al-Otaibi, 2011), paper (Jiang et al., 2004), and bacterial cellulose (Jung, Kim, Kim, & Jin, 2009; Maneerung et al., 2008). In those works, silver cations were adsorbed onto the solids then reduced to nanoparticles with added reducing reagents either with or without stabilizing chemicals. For instance, the bound silver cations on cotton fabrics were reduced by basic aqueous glucose solution with cetyltrimethylammonium bromide (El-Shishtawy, et al., 2011) and those on cellulose acetate aerogels (Luong, Lee, & Nam, 2008) and bacteria cellulose (Jung et al., 2009) were reduced by sodium borohydride to AgNPs to demonstrate anti-microbial properties. However, none showed evidence of actual binding nor persistence of AgNPs on the surfaces.

The goal of this work was to use alkali lignin (AL) as a multi-functional agent to bind onto cellulose fiber surfaces, complex with silver anions, reduce them to atomic silver toward growing into nanoparticles as well as cap the surface bound nanoparticles. The use of lignin is advantageous in several aspects. Lignin is non-toxic to human and also environmentally benign, offering a "green" approach. Lignin is the second most abundantly macromolecule only after cellulose, thus readily available. Lignin is not only tightly associated with cellulose in plant cells but model lignin molecules also have shown to exhibit high affinity to cellulose through polar interactions between their hydroxyl groups as well as hydrophobic interactions between the lignin phenyl rings and cellulose backbones in a computational study (Houtman & Atalla, 1995). The large intra- and inter-molecular spacings in the

* Corresponding author. Tel.: +1 530 752 0843.
*E-mail address:* ylhsieh@ucdavis.edu (Y.-L. Hsieh).

http://dx.doi.org/10.1016/j.carbpol.2015.05.060
0144-8617/

heterogeneous polyphenolic structures of lignin have also shown to be capable of binding and complexing with silver cations via cation-hydroxyl and cation-π bonding (Lagutschenkov, Sinha, Maitre, & Dopfer, 2010). Additionally, the bound silver cations can be reduced by the phenolic hydroxyls to grow into zero-covalent nanoparticles (Sivaraman, Elango, Kumar, & Santhanam, 2009). These individually demonstrated abilities of lignin were deemed feasible for lignin to serve as multi-functional reagent to bind cellulose, complex with silver cations and to reduce them to atomic silver and then silver nanoparticles (AgNPs), facilitating multiple processes in an efficient manner. Bound lignin may create additional functional properties such as anti-microbial and UV absorbing activities to cellulose as Kraft lignins derived from bagass and cotton stalk have exhibited antimicrobial activities towards Bacillus subtilis and Bacillus mycoid (Nada, Eldiwany, & Elshafei, 1989) and lignin molecules have shown to absorb lights at UV–Vis region (Pearl, 1967). Furthermore, the known thermal stability of lignin may also improve that of cellulose.

## 2. Experiment

### 2.1. Chemicals

Alkali lignin (AL) ($M_w$ = 28 kDa, spruce origin, Sigma-Aldrich), alkali lignin (low sulfonate) ($AL_{ls}$) ($M_w$ = 60 kDa, spruce origin, Sigma-Aldrich), sodium hydroxide (NaOH, 85%, EM Science), hydrochloric acid (HCl, 37 wt%, Fisher Scientific), sodium borohydride ($NaBH_4$, practical grade, Fisher Scientific) and silver nitrate ($AgNO_3$, practical grade, Acros Organic) were used as received. Water used was purified by Milli-Q plus water purification system (Millipore Corporate, Billerica, MA). Cellulose (Cell) fibrous membranes were prepared by electrospinning of cellulose acetate in 2:1 acetone:DMAc co-solvents followed by deacetylation via aqueous hydrolysis (Liu & Hsieh, 2002).

### 2.2. Solubility of AL in alkali aqueous solutions

AL was added to aqueous NaOH of varying concentrations between 0.5 and 5 wt% to prepare 40 wt% AL colloidal solutions, stirred for 24 h, then centrifuged (Centrifuge 5804R, Eppendorf) for 10 min at 5000 rpm. 5 g of the supernatant were neutralized with 5 wt% hydrochloric acid to precipitate AL, clearing the solution. The precipitated AL was washed with deionized water repeatedly, dried at 60 °C for 24 h, then weighed to calculate the solubility of lignin:

$$\text{Solubility (wt\%)} = \frac{\text{Precipited lignin (g)}}{5\,\text{(g)}} \times 100\,\text{wt\%} \quad (1)$$

### 2.3. Preparation of AL-Cell and AgNPs–AL-Cells

Cell was immersed in 15 wt% AL in 1 wt% NaOH aqueous solution at 80 °C for 30 min. AL bounded Cell (AL-Cell) was then thoroughly rinsed with water at ambient temperature once and then at boil three times when the final rinse was clear and then dried in oven at 60 °C for 24 h. Silver nanoparticles (NPs) were then synthesized on AL-Cell by immersing the membrane in 20 mmol/L silver nitrate solution under gentle stirring at boil for 5 or 10 min to obtain AgNPs–AL-Cell 5 and 10. The AgNPs–AL-Cells were then thoroughly rinsed by deionized water then dried and kept in a dessicator for further characterization. In order to examine the binding strength of the AgNPs on AL-Cells, 10 mg of the dried AgNPs–AL-Cell 10 was dispersed in 5 mL of 0.04 wt% $AL_{ls}$ aqueous solutions and sonifcated (Sonicator S-4000, Misonix) at 80 amplitude (80 to 90 watts) for 10 and 30 min. $AL_{ls}$ was used as the dispersing reagents to cap and stabilize the AgNPs that could possibly be shaken off the cellulose nanofibrous membrane after strong sonification. The suspensions then were then centrifuged at 5000 rpm for 30 min and the supernatant were decanted and kept for further characterization.

### 2.4. Preparation of AgNPs-Cells control samples

In order to validate the superiority of our experiment design, two control samples were prepared via different approaches. The first control sample was prepared by placing Cell directly in 20 mmol/L silver nitrate solution at boiling temperature under gentle stirring for 10 min to prepare AgNPs-Cell a. The second control sample was synthesized by immersing Cell in 20 mmol/L silver nitrate solution under gentle stirring for 6 h, and then thoroughly rinsed with water three times followed by drying in oven at 60 °C for 1 h. The dried sample was then immersed in 10 mmol/L sodium borohydride solution under gentle stirring for 10 min to obtain silver nanoparticles coated Cell (AgNPs-Cell b). Both the AgNPs-Cell control samples were then thoroughly rinsed by deionized water then dried and kept in a dessicator for further characterization.

### 2.5. Antibacterial test

The antibacterial property was tested against gram-negative bacteria, *Escherichia coli* (K-12) based on modified AATCC test method 100. The bacteria were cultured in Luria broth under aerobic conditions at 37 °C for 24 h. Both Cell and AgNPs–AL-Cell 10 weighed 0.2 g were placed in separate sterilized jars containing 30 mL $10^5$ colony forming unit (CFU)/mL bacterial suspension for 10 min. Then an aliquot of 0.1 mL solution was taken out for serial dilutions to be placed on one of the four quadroon of an agar plate and incubated at 37 °C for 24 h. The inhibition zone was also evaluated by placing four AgNPs–AL-Cell 10 samples, each in 0.8 cm × 1 cm size, in a sterile agar plate, then an aliquot of 0.1 mL $10^5$ CFU/mL bacterial were evenly spread on it and incubated at 37 °C for 24 h.

### 2.6. Analytical methods

The chemical structures of AL were examined by Fourier transform infrared spectroscopy (FTIR) (Nicolet 6700, Thermo Scientific). The FTIR spectrum was collected from samples mixed and pressed with anhydrous KBr powders into pallets. The optical properties of AL solutions, Cell, AL-Cell and AgNPs–AL-Cell suspensions, as well as the supernatant solutions from AgNPs–AL-Cell suspension after strong sonification were examined by ultraviolet-visible spectroscopy (UV–vis) (Evolution 600, Thermo Scientific). Aqueous AL solutions at 0.001 to 0.005 wt% in 1 wt% NaOH were measured. Aqueous suspensions of Cell, AL-Cell and AgNPs–AL-Cell were prepared by placing the membrane in deionized water at 0.5 g/L concentration and then mildly sonicated at 40 amplitude (40–50 W) for 5 min (Sonicator S-4000, Misonix). The solutions were placed in quartz cuvettes with 1-cm path length for UV–vis measurements. The color and reflectance spectrum of Cell, AL-Cell and AgNPs–AL-Cell were characterized by a colorimeter (Color-eye 7000 A, GretagMacbeth). A 4 × 4 cm thin piece of each sample was cut by scissor for the colorimeter measurement. The morphology and structure of Cell, AL-Cell and AgNPs–AL-Cell were observed by stereo microscopy (EZ 40, Leica), scanning electron microscopy (SEM) (FEI-XL 30, FEI) and transmission electron microscopy (TEM) (JEOL 3000, JEOL). The samples were observed directly under stereomicroscope with 8× magnification. SEM samples were sputter coated with gold for 1 min and observed under a working voltage of 5 kV. TEM samples were prepared by placing a drop of the dilute (ca 0.02 g/L) mildly sonicated suspension onto a carbon grid, then letting dry in air. The atomic compositions of crude AgNPs–AL-Cells were carried out by energy-dispersive X-ray spectroscopy (EDX) adjunct to SEM. A small piece of AgNPs–AL-Cells were placed

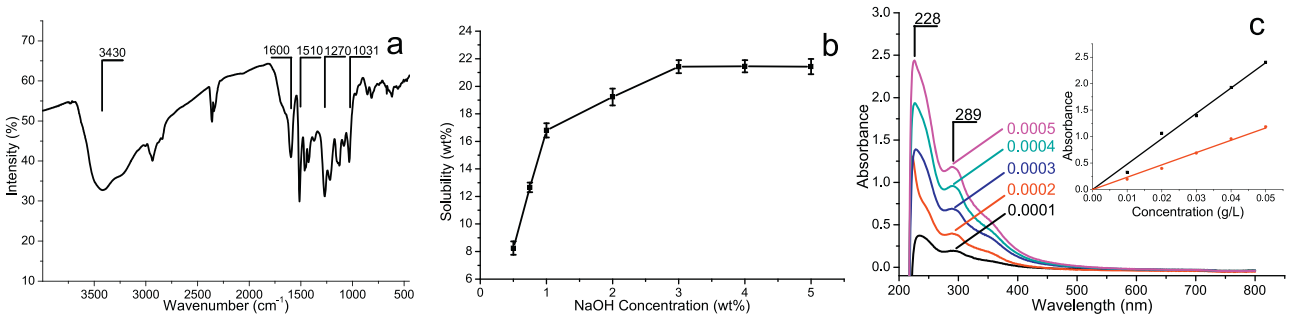


**Fig. 1.** Alkali lignin (a) FTIR; (b) solubility in aqueous NaOH solutions; (c) UV–vis of 0.0001 to 0.0005 wt% lignin in 1 wt% NaOH aqueous solution. Inset figure in (c) absorbance at 228 (black line) and 289 (red line) nm. (For interpretation of the references to color in this figure legend, the reader is referred to the web version of this article.)

on carbon tape on aluminum support and dried in oven at 60 °C for 24 h before EDX measurements. Zeta potential of Cell, AL-Cell and AgNPs–AL-Cells were characterized by Zetasizer (Nano ZS 90, Malvern). All the samples (0.02 g/L) were mildly sonicated at 40 amplitude for 5 min before zeta potential analysis. The thermal properties of Cell AL-Cell and AgNPs–AL-Cells were analyzed by differential scanning calorimeter (DSC) (DSC-60, Shimadzu) and thermogravimetric analysis (TGA) (TGA-50, Shimadzu). All DSC and TGA samples were dried in oven at 60 °C for 24 h before characterization. DSC samples, tightly packed in aluminum pans, covered and press-sealed, were heated at 10 °C/min under a 30 mL/min $N_2$ flow to 550 °C. TGA samples were heated at 10 °C/min to 550 °C under a 50 mL/min $N_2$ flow. The AgNPs–AL-Cell 10 in particular was heated to 180 °C and held for 60 min and cooled back to ambient temperature to study the sintering behavior of silver nanoparticles.

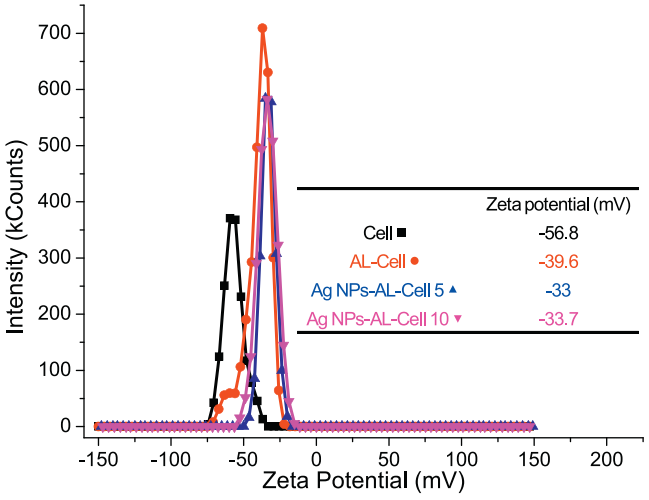


**Fig. 2.** Zeta potentials of Cell, AL-Cell and AgNPs–AL-Cells.

## 3. Results and discussion

### 3.1. AL structure and solubility

The FTIR spectrum of AL (Fig. 1a) clear lignin characteristic peaks: phenolic and aliphatic hydroxyls at around 3430 $cm^{-1}$, two minor asymmetric —$CH_2$ at 2930 $cm^{-1}$ and symmetric —$CH_3$ stretching peaks at 2835 $cm^{-1}$, aromatic skeletal vibration peaks around 1600 and 1513 $cm^{-1}$, aromatic C—H in plane deformation peak at 1130 $cm^{-1}$ as well as aromatic ring breathing with C=O groups at 1270 $cm^{-1}$. The two distinctive peaks at 1081 and 1031 $cm^{-1}$ caused by the C—O deformation suggested the presence of primary and secondary alcohols on the lignin phenylpropanoid side chains, as well as the characteristic peak at 1650 $cm^{-1}$ for the various intramolecular ether linkages and γ-lactone ring.

The highly crosslinked and hydrophobic phenylpropanoid structure of AL renders it water insoluble under the neural condition. However, AL can be made aqueous soluble when the phenolic hydroxyl groups are ionized under basic conditions. The solubility of AL increased with increasing base concentrations, plateauing at 21.4 wt% at 3 wt% NaOH and above (Fig. 1b), showing optimal ionization of the AL phenolic hydroxyls into phenolate ions to be soluble at and above 3 wt% NaOH.

The UV–vis spectrum of AL showed absorbance mostly in the UVC (100 nm to 280 nm) and UVB (280 nm to 315 nm) regions but much less in the UVA (315 nm to 400 nm) range (Fig. 2). The major peak at 228 nm and secondary peak at 289 nm corresponded to the respective $E_2$ band (intermediate energy) and B band (lowest energy) associated with the π to π* transition of lignin phenylpropanoid structures, both intensified with increasing AL concentrations. The weight extinction coefficients, determined via Beer–Lambert Law (Eq. (2)), were 47.9 ± 1.1 and 23.3 ± 0.5 L/g/cm at 228 nm and 289 nm, respectively, granting AL moderately UV absorbing ability comparing to the 80 to 150 L/g/cm values reported on common UV absorbing dyes (Hirayama, 1967).

$$A = \left(\frac{\mu}{\rho}\right) \times \rho \times l \quad (2)$$

$\mu/\rho$ is the weight extinction coefficient; $\rho$ is the solution density; $l$ is the path length of the light beam.

### 3.2. Role and binding of AL to cell

Alkali lignin bound cellulose (Al-Cell) was prepared by immersing cellulose fibrous membranes in basic AL solutions, then thoroughly rinse with water to remove loosely bound lignin. To maximize lignin content with minimal alkali, 15 wt% AL aqueous solution in 1 wt% NaOH was used. The rinsed AL-Cell was then immersed in 20 mmol/L silver nitrate solution at boil. The silver nitrate solutions remained clear, showing no AL leaching and confirming AL to be firmly bounded to the cellulose fiber surfaces.

The controlled samples were prepared without AL immersions: AgNPs-Cell a was Cell immersed in silver nitrate then, while control sample AgNPs-Cell b was Cell immersed in silver nitrate then reduced by sodium borohydrid. Both control samples were white in color as the original Cell shown by their microscope images (Fig. S1). The color coordinates (Table 1) of AgNPs-Cell a and b showed slight decreases in lightness L by 1.89 and 3.94, respectively, while the red color index a increased by 0.26 and 0.55 and yellow color index b increased by 2.31 and 3.47, respectively, confirming their slight yellow to red colors and no evidence of silver nanoparticles on Cell in absence of AL. In control sample a, the original Cell lacking reducing groups did not support the growth of nanoparticles even with

**Table 1**
Color coordinates of Cell, AgNPs-Cell a and b.

| | Cell | AgNPs-Cell a | AgNPs-Cell b |
|---|---|---|---|
| $L$ | 98.0 | 96.11 | 94.06 |
| $a$ | −0.13 | 0.03 | 0.42 |
| $b$ | 0.03 | 2.34 | 3.50 |
| $\Delta L$ | None | −1.89 | −3.94 |
| $\Delta a$ | None | 0.16 | 0.39 |
| $\Delta b$ | None | 2.31 | 3.47 |

excessive silver cations. In control sample b, silver cations bound on negatively charged groups on original Cell could be reduced by sodium borohydride into single silver atoms, but could not grow into silver nanoparticles due to their spatial separation on cellulose fiber surfaces. The above observations demonstrated that, without AL, neither control samples could support the formation nor growth of AgNPs, confirming the essential roles of AL as the binding, complexing and reducing reagents in silver nanoparticle synthesis on these cellulose membranes.

### 3.3. Surface charge

The surface charge properties of Cell, AL-Cell and AgNPs–AL-Cells were characterized by their zeta potential (Fig. 2). Cell showed a zeta potential of −56.8 mV which is consistent with the negatively charged cellulose surfaces. AL modified cellulose or AL-Cell was less negatively charged with a zeta potential of −39.6 mV, indicating partly covered fiber surfaces with the less negatively charged lignin, evident by the low p*K*a of lignin phenolic hydroxyls. Following reduction, the negatively charges on AgNPs–AL-Cell 5 and 10 were further lowered to −33 and 33.7 mV, respectively. The decrease of negatively charged groups on the fiber surfaces could be due to a combination of oxidation of lignin phenolic hydroxyls by silver cations and presence of subsequently formed silver nanoparticles on the surfaces. Ag NPs-AL-Cell 5 and 10 showed nearly identical surface charges, implying silver cations to be reduced on the existing silver atomic clusters or nanoparticles on AL-Cell grew into bigger nanoparticles as reaction time increased (Suber, Sondi, Matijević, & Goia, 2005).

### 3.4. Optical properties

As shown by the stereomicroscope, Cell appeared white, AL-Cell was brown-grey and AgNPs–AL-Cells were light to dark yellow (Fig. 3). The color quality of AL-Cell was further detailed by colorimetric measurements, i.e., reduced lightness ($\Delta L = -12.8$), but increased redness ($\Delta a = 2.66$) and yellowness ($\Delta b = 12.06$). This clearly indicates the presence of AL in Cell fibrous membrane. The AgNPs–AL-Cells were light (5 min) and dark (10 min) yellow-brown in colors. The color coordinates showed decreasing lightless L from 85.2 of Al-Cell to 83.05 and 80.62, for AgNPs–AL-Cell5 and AgNPs–AL-Cell10, respectively. However, the red color index $a$ decreased from 2.53 to 0.73 while yellow color index $b$ increased from 12.09 to 16.11 from the 5 min reaction, consistent with the light yellow color. After 10 min reaction time, both red and yellow color indexes increased from 0.73 to 3.22 and from 16.11 to 22.38, respectively, showing darkened yellowness.

The above observation clearly showed that AL could sufficiently cover Cell fiber surfaces and the surface bound AL could effectively complex with sufficient silver cations within lignin intra- and inter-molecular spaces, allowing the reduced single silver atoms to coalesce into nanoparticles.

Cell exhibited 95% colorimetric reflectance over the entire visible region, consistent with its white color. AL-Cell showed decreasing reflectance of 83% at 750 nm to 35% at 350 nm, showing visible light absorption by AL, especially in purple and blue regions. AgNPs–AL-Cells exhibited strong absorptions centering around low 400 nm region, reflecting a combination of color absorption of lignin and the surface plasmon resonance of the silver nanoparticles (Fig. 4a). The peak around 420 nm increased in intensity and slightly red shifted with increasing reaction time, consistent with the growth of AgNPs in sizes and quantities (Kelly, Coronado, Zhao, & Schatz, 2003). In the UV–vis spectra of supernatants from strongly sonicated AgNPs–AL-Cells 10 in 0.04 wt% $AL_{ls}$ aqueous solutions showed no silver NP characteristic peaks. In fact, UV–vis spectra of AgNPs supernatant from 10 and 30 min sonification were not distinguishable from that of the 0.04 wt% $AL_{ls}$ aqueous control sample, showing no detectable AgNPs in the supernatants and confirming AgNPs to be very tightly bound to AL-Cells.

In the UV–vis spectra of Cell, AL-Cell, and AgNPs–AL-Cell suspensions (Fig. 4b), Cell showed little absorbance while AL-Cell showed

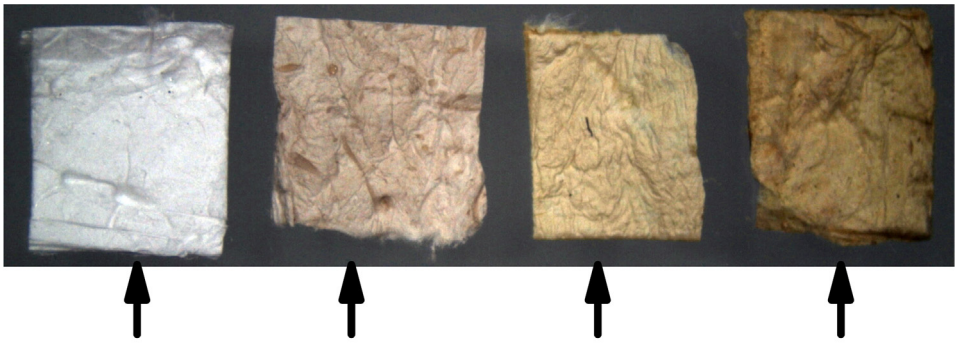

| | Cell | AL-Cell | Ag NPs-AL-Cell 5 | Ag NPs-AL-Cell 10 |
|---|---|---|---|---|
| L | 98.0 | 85.2 | 83.05 | 80.62 |
| a | -0.13 | 2.53 | 0.73 | 3.22 |
| b | 0.03 | 12.09 | 16.11 | 22.38 |
| ΔL | none | -12.8 | -14.95 | -17.38 |
| Δa | none | 2.66 | 0.86 | 3.35 |
| Δb | none | 12.06 | 16.08 | 22.35 |

**Fig. 3.** Stereo microscope images and color coordinates of Cell, AL-Cell and AgNPs–AL-Cell 5 and 10.

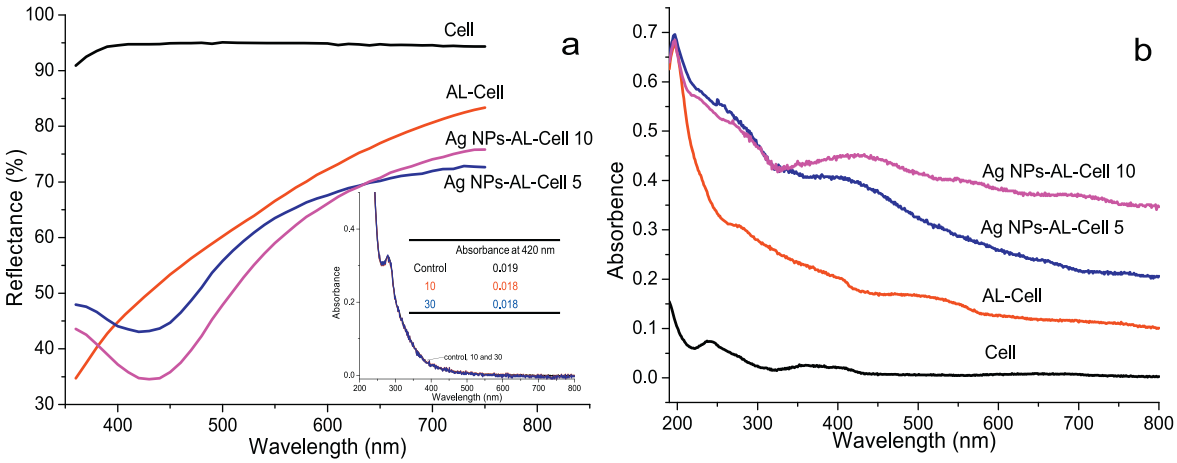


**Fig. 4.** (a) Reflectance spectrum and (b) UV–vis spectrum of AL-Cell and AgNPs–AL-Cells, Inserted figure in (a): UV–vis spectrum of supernantant from AgNPs–AL-Cell 10 in 0.04 wt% $AL_{IS}$ aqueous solutions after up to 30 min strong sonification.

an intense peak at 197 nm in the UVA region as well as a large broad shoulder over the UVB and UVC regions, a clear evidence of lignin phenylpropanoid structures and the presence of AL. AgNPs–AL-Cells showed similar absorbance activities as AL-Cell in UVB and UVC regions as well, i.e., sharp peaks at 197 nm and wide shoulder from 210 to 325 nm. Meanwhile, broad peaks near 415 and 430 nm were observed for AgNPs–AL-Cell 5 and AgNPs–AL-Cell 10, respectively, characteristic of surface plasmon resonance of AgNPs. These results well correlated to reflectance spectrum of their solid thin film (Fig. 4a). Since AL-Cell and AgNPs–AL-Cell samples were sonicated prior to UV–vis measurements, the above UV observations again confirmed excellent binding of both AL and AgNPs on Cell.

The stereomicroscope and colorimeter results (Fig. 3) have provided visual evidence of the successful binding of AL on cellulose, as well as subsequent AgNP formation on Cell. Colorimeter reflectance and UV–vis absorbance spectrum of AL-Cell exhibited a broad absorption with decreasing intensity as the wavelength increased from UVC to blue light region. AgNPs–AL-Cells showed similar absorption in UVB and UVC regions, again evident of the UV absorbing ability, as well as peaks around 420 nm, clearly indicating the presence of AgNPs.

### 3.5. Morphology of Cell membranes and AgNPs

The SEM image showed Cell fibrous membrane to consist of 50 nm to ~1 μm wide fibers in twisted ribbon or cylindrical shapes with smooth surfaces (Fig. S2a). AL-Cell appeared very similar to Cell (Fig. S2b), indicating no structural effect from AL binding. More importantly, the absence of any AL particles or aggregates on or between fibers indicates AL to be uniformly distributed and bound to fiber surfaces. AgNPs–AL-Cells (Fig. S2c and d) also maintained the fibrous structures and sizes as well, showing few nanparticles on AgNPs–AL-Cell 5 (Fig. S2c), but numerous nanoparticles on AgNPs–AL-Cell 10 surfaces (Fig. S2d).

The presence of AgNPs was more clearly shown by TEM and EDX mapping (Fig. 5). AgNPs–AL-Cell 5 (Fig. 5a) showed small spherical AgNPs with rather uniform sizes of less 5 nm on the fiber surfaces. All AgNPs were covered with very thin, i.e., less than 2 nm thick, layers of electron transparent organics, presumably lignin (Fig. S3). Since these samples were sonicated prior to TEM imaging, these above observations confirmed these AgNPs to be stably bound to the fiber surfaces. The EDX spectrum of AgNPs–AL-Cell 5 showed 46.2 wt% or 55 at% C and 53.8 wt% of 45 at% O (Fig. 5b), essentially identical to the theoretical 55.5 at% C and 44.5 at% O compositions of cellulose. The quantity of silver on of AgNPs–AL-Cell 5 was below the detectable level of EDX. A much larger number of AgNPs with sizes varying from 4 to 100 nm were observed on AgNPs–AL-Cell 10 (Fig. 5c). Silver was detected by EDX at 2.9 wt% (Fig. 5c) and distributed evenly on AgNPs–AL-Cell 10 (Fig. 5e), whose C and O compositions were 48.5 wt%/56.9 at% and 48.6 wt%/42.8 at%, respectively, also close to the theoretic C and O compositions of cellulose.

The Ag nanoparticle size, number & distribution density seemed to positively correlate to reaction time and fiber sizes as smaller ca. 15 nm diameter AgNPs were observed on 300 nm wide fibers and larger ca. 80 nm AgNPs were found on larger 500 nm wide fibers. Silver nanoparticles could grow in sizes with longer synthesis time whereas larger AgNPs on larger fibers could be due the closer proximity of bulky lignin molecules, increasing local concentrations of silver cations and atoms and subsequently larger AgNPs. The electron microscopic observations confirmed lignin to be very efficient binder for cellulose and $Ag^+$, reducer for $Ag^+$ to synthesize Cell bound AgNPs as well as effective capping reagent to stably immbolize AgNPs on cellulose fiber surfaces.

### 3.6. Thermal properties

Both Cell and AL showed similar hygroscopic moisture loss near 100 °C and onset of thermal decomposition at 200 °C. Cell showed two decomposition exotherms at 320 and 433 °C, corresponding the rapid mass loss to 18.5 wt% at 370 °C and to 4.15 wt% at 550 °C, respectively (Fig. 6). The first exotherm is from cellulose decomposition, while the second one is due to charring. AL showed only one major exotherm at 475 °C, corresponding much stable thermal stability with gradual mass loss to 56.1% at 550 °C. Adsorption of AL on Cell raised the onset decomposition to 275 °C, and the cellulose decomposition exotherms to 330 and 495 °C, leaving 8.4% residue at 550 °C. Both AgNPs–AL-Cell s had similar thermal decomposition onset at 250 °C, higher than both Cell and AL, to leave less than 5% at 550 °C. The lower residual char from AgNPs–AL-Cell s than AL-Cell may imply facilitated decomposition of cellulose and lignin from possible redox reactions between silver nanoparticles and the oxidative species generated during lignocellulosic pyrolysis, another indication of strong binding between silver nanoparticles and Cell substrate. Although the thermal behaviors of AgNPs–AL-Cells were not significantly different from Cell, AgNPs on Cell capped by lignin remained un-agglomerated even after prolonged heating at 180 °C (Fig. 6c), indicating much improved thermal stability over isolated AgNPs which would sinter and melt below 150 °C (Moon et al., 2005). Therefore, not only Cell-bound AgNPs

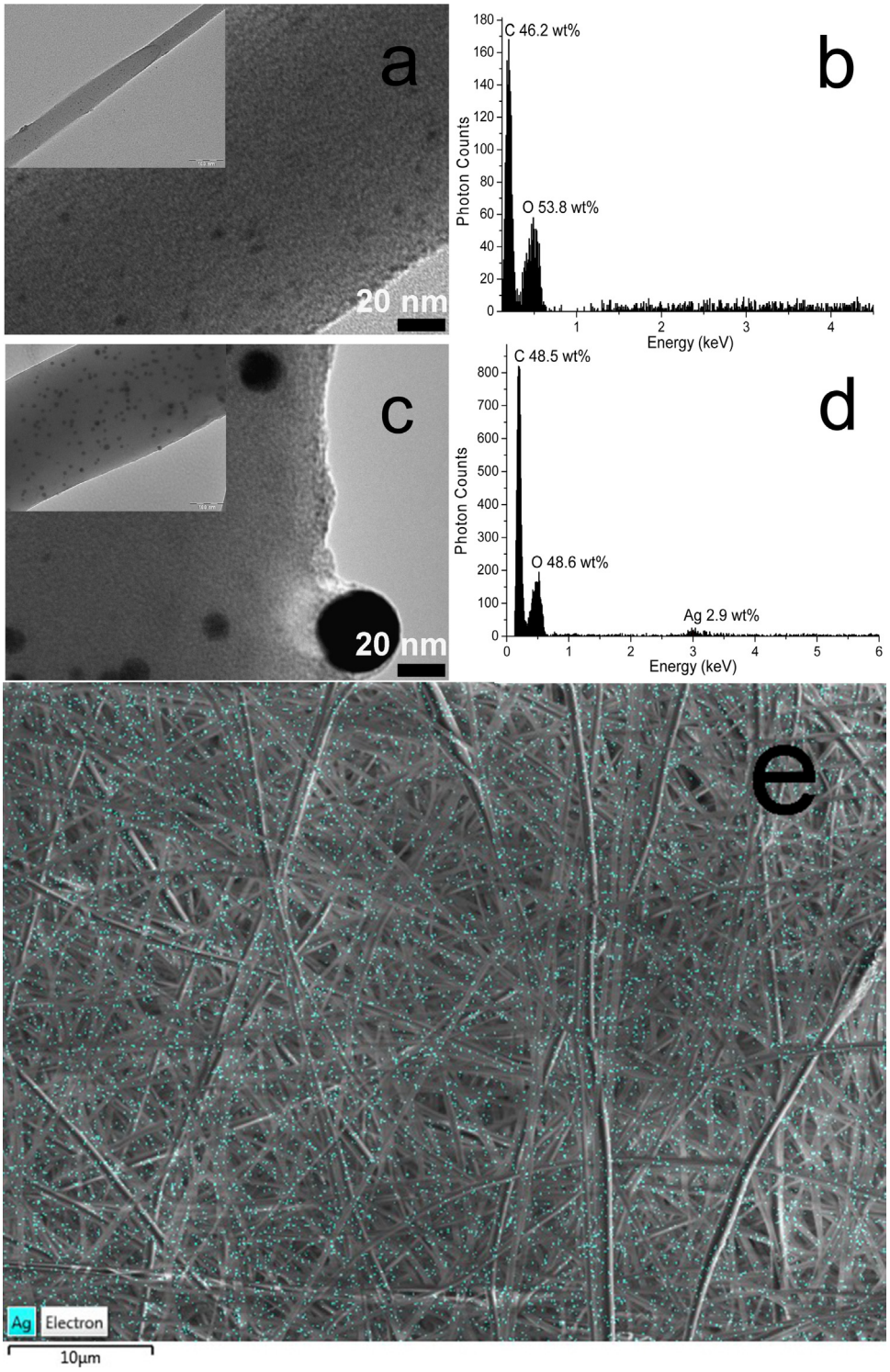


**Fig. 5.** TEM and EDX of AgNPs–AL-Cell 5 (a and b); 10 (c and d); (d) elemental mapping of Ag on AgNPs–AL-Cell 10.

are more thermally stable but their tendency to agglomerate is also effectively prevented.

### 3.7. Antibacterial properties

Incubation of the *E. coli* suspension exposed to the original unmodified Cell clearly showed colony growth on the agar plate (Fig. 7a), while that exposed to AgNPs–AL-Cell 10 for only 10 min showed no bacterial growth at all (Fig. 7b), indicating complete inhibition of cell viability. Such brevity in exposure shows effective antibacterial properties of the Cell bounded AgNPs against *E. coli* in suspensions. When exposed on the agar plate, inhibition of *E. coli* growth was also evident. The inhibition zone or diameter around the 8 mm by 10 mm size AgNPs–AL-Cell 10 samples was ca. 3 mm (Fig. 7c). Although the antibacterial mechanism of AgNPs against bacteria is not entirely understood, hypotheses have been proposed. Oxidative stress induced by the free radicals generated could disrupt the membrane of bacteria that are in contact with (Hajipour

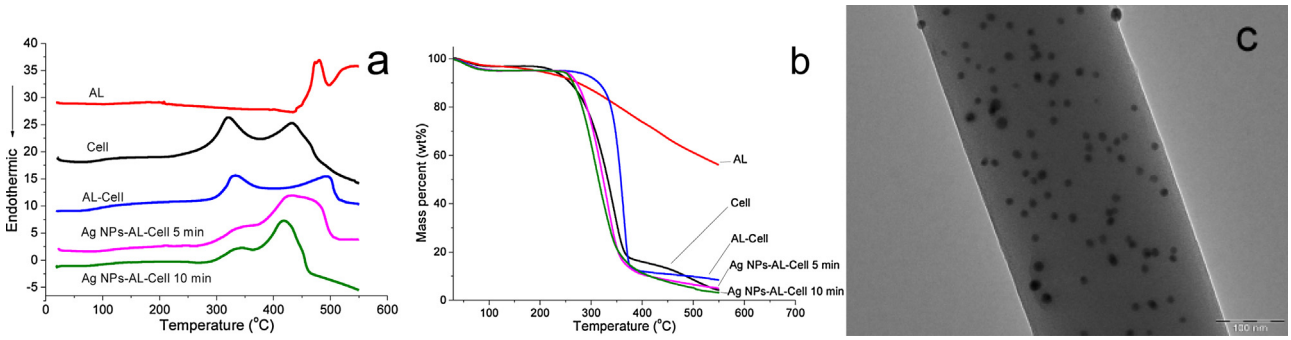


**Fig. 6.** (a) DSC and (b) TGA of AL, Cell, AL-Cell, AgNPs–AL-Cells. (c) TEM of AgNPs–AL-Cell 10 after heating to 180 °C for 60 min.

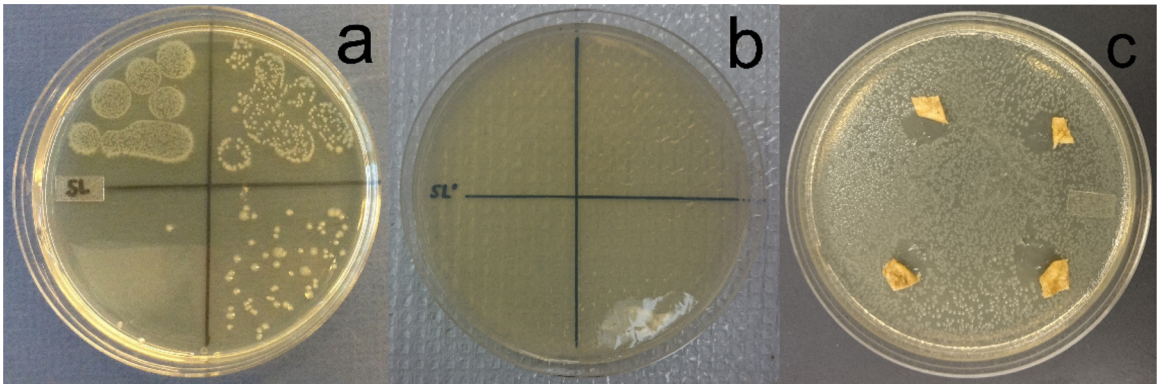


**Fig. 7.** Photograph of incubated (37 °C, 24 h) agar plates containing aliquots of four serial diluted *Escherichia coli* suspensions exposed for 10 min to: (a) Cell; (b) AgNPs–AL-Cell 10; (c) inhibition zone around membranes with 0.1 mL $10^5$ CFU/mL *E. coli*.

et al., 2012). Silver ions could also be released from AgNPs to disrupt the bacteria membrane integrity via electrostatic interaction (Chernousova & Epple, 2013), leading to an inhibition zone around the swatch. The relatively limited zones seem to reflect the limited contact and/or diffusion of either the free radicals or ions under the more static condition of agar plate. These observations are not only consistent with the fact that AgNPs are tightly bound to cellulose fiber surfaces, but also capped by lignin layer.

## 4. Conclusion

Alkali lignin has been demonstrated to be highly effective multifunctional binding, complexing, reducing and capping reagents for silver nanoparticle synthesis on electrospun cellulose fibrous membranes. The synthesis procedure was simple and efficient, requiring only 10 min reaction times to achieve a 2.9% AgNP loading. The AgNP bounded cellulose fibrous membranes appeared yellow and exhibited characteristic silver nanoparticle surface resonance peaks around 420 nm in both UV–vis absorption and colorimeter reflectance spectrum. The synthesized AgNPs remained on lignin modified cellulose fiber surfaces, showing no detactable nanoparticles in the rinsing solutions following sonication. The spherical AgNPs were evenly distributed on fiber surfaces, without aggregation, and clearly capped by ca. 2 nm thick lignin layer. The sizes and quantities of AgNPs correlated positively to both fiber sizes and length of synthesis time. The presence of lignin on cellulose fibers conferred UV absorbing ability in both UV-B and UV-C regions and much improved thermal stability. The AgNPs bound to lignin-modified cellulose remained isolated from each other, showing no agglomeration when exposed to elevated temperatures. AgNPs–AL-Cell 10 exhibited 100% reduction of *E. coli* inoculated with $10^5$ CFU/mL after only 10 min contact time, with a 3 mm inhibition zone, demonstrating excellent antibacterial properties against *E. coli*.

## Appendix A. Supplementary data

Supplementary data associated with this article can be found, in the online version, at http://dx.doi.org/10.1016/j.carbpol.2015.05.060

## References

AshaRani, P. V., Mun, G. L. K., Hande, M. P., & Valiyaveettil, S. (2009). Cytotoxicity and genotoxicity of silver nanoparticles in human cells. *ACS Nano*, *3*(2), 279–290.

Batchelor-McAuley, C., Tschulik, K., Neumann, C. C., Laborda, E., & Compton, R. G. (2014). Why are silver nanoparticles more toxic than bulk silver? Towards understanding the dissolution and toxicity of silver nanoparticles. *International Journal of Electrochemical Science*, *9*, 1132–1138.

Ben-Sasson, M., Lu, X., Bar-Zeev, E., Zodrow, K. R., Nejati, S., Qi, G., et al. (2014). In situ formation of silver nanoparticles on thin-film composite reverse osmosis membranes for biofouling mitigation. *Water Research*, *62*, 260–270.

Chernousova, S., & Epple, M. (2013). Silver as antibacterial agent: Ion, nanoparticle, and metal. *Angewandte Chemie International Edition*, *52*(6), 1636–1653.

El-Shishtawy, R. M., Asiri, A. M., Abdelwahed, N. A. M., & Al-Otaibi, M. M. (2011). In situ production of silver nanoparticle on cotton fabric and its antimicrobial evaluation. *Cellulose*, *18*(1), 75–82.

Gliga, A. R., Skoglund, S., Wallinder, I. O., Fadeel, B., & Karlsson, H. L. (2014). Size-dependent cytotoxicity of silver nanoparticles in human lung cells: The role of cellular uptake, agglomeration and Ag release. *Particle and Fibre Toxicology*, *11*, 11.

Hajipour, M. J., Fromm, K. M., Ashkarran, A. A., de Aberasturi, D. J., de Larramendi, I. R., Rojo, T., et al. (2012). Antibacterial properties of nanoparticles. *Trends in Biotechnology*, *30*(10), 499–511.

Hirayama, K. (1967). *Handbook of ultraviolet and visible absorption spectra of organic compounds*. New York, NY: Plenum Press Data Division.

Houtman, C. J., & Atalla, R. H. (1995). Cellulose-lignin interactions (A computational study). *Plant Physiology*, *107*(3), 977–984.

Jiang, H. Q., Manolache, S., Wong, A. C. L., & Denes, F. S. (2004). Plasma-enhanced deposition of silver nanoparticles onto polymer and metal surfaces for the generation of antimicrobial characteristics. *Journal of Applied Polymer Science*, *93*(3), 1411–1422.

Jung, R., Kim, Y., Kim, H. S., & Jin, H. J. (2009). Antimicrobial properties of hydrated cellulose membranes with silver nanoparticles. *Journal of Biomaterials Science-Polymer Edition*, *20*(3), 311–324.

Kelly, K. L., Coronado, E., Zhao, L. L., & Schatz, G. C. (2003). The optical properties of metal nanoparticles: The influence of size, shape, and dielectric environment. *Journal of Physical Chemistry B*, *107*(3), 668–677.

Kim, J. S., Kuk, E., Yu, K. N., Kim, J. H., Park, S. J., Lee, H. J., et al. (2007). Antimicrobial effects of silver nanoparticles. *Nanomedicine-Nanotechnology Biology and Medicine*, *3*(1), 95–101.

Lagutschenkov, A., Sinha, R. K., Maitre, P., & Dopfer, O. (2010). Structure and infrared spectrum of the Ag+-phenol ionic complex. *Journal of Physical Chemistry A*, *114*(42), 11053–11059.

Li, Y., Leung, P., Yao, L., Song, Q. W., & Newton, E. (2006). Antimicrobial effect of surgical masks coated with nanoparticles. *Journal of Hospital Infection*, *62*(1), 58–63.

Liu, H. Q., & Hsieh, Y. L. (2002). Ultrafine fibrous cellulose membranes from electrospinning of cellulose acetate. *Journal of Polymer Science, B—Polymer Physics*, *40*(18), 2119–2129.

Lok, C. N., Ho, C. M., Chen, R., He, Q. Y., Yu, W. Y., Sun, H., et al. (2007). Silver nanoparticles: Partial oxidation and antibacterial activities. *Journal of Biological Inorganic Chemistry*, *12*(4), 527–534.

Luong, N. D., Lee, Y., & Nam, J. D. (2008). Highly-loaded silver nanoparticles in ultrafine cellulose acetate nanofibrillar aerogel. *European Polymer Journal*, *44*(10), 3116–3121.

Maneerung, T., Tokura, S., & Rujiravanit, R. (2008). Impregnation of silver nanoparticles into bacterial cellulose for antimicrobial wound dressing. *Carbohydrate Polymers*, *72*(1), 43–51.

Moon, K.-S., Dong, H., Maric, R., Pothukuchi, S., Hunt, A., Li, Y., et al. (2005). Thermal behavior of silver nanoparticles for low-temperature interconnect applications. *Journal of Electronic Materials*, *34*(2), 168–175.

Nada, A. M. A., Eldiwany, A. I., & Elshafei, A. M. (1989). Infrared and antimicrobial studies on different lignins. *Acta Biotechnologica*, *9*(3), 295–298.

Pearl, I. A. (1967). In Irwin A. Pearl (Ed.), *The chemistry of lignin* (pp. 1–35). London: Dekker.

Sivaraman, S. K., Elango, I., Kumar, S., & Santhanam, V. (2009). A green protocol for room temperature synthesis of silver nanoparticles in seconds. *Current Science*, *97*(7), 1055–1059.

Suber, L., Sondi, I., Matijević, E., & Goia, D. V. (2005). Preparation and the mechanisms of formation of silver particles of different morphologies in homogeneous solutions. *Journal of Colloid and Interface Science*, *288*(2), 489–495.

Sun, Y. G., & Xia, Y. N. (2002a). Large-scale synthesis of uniform silver nanowires through a soft, self-seeding, polyol process. *Advanced Materials*, *14*(11), 833–837.

Sun, Y. G., & Xia, Y. N. (2002b). Shape-controlled synthesis of gold and silver nanoparticles. *Science*, *298*(5601), 2176–2179.

Taglietti, A., Arciola, C. R., D'Agostino, A., Dacarro, G., Montanaro, L., Campoccia, D., et al. (2014). Antibiofilm activity of a monolayer of silver nanoparticles anchored to an amino-silanized glass surface. *Biomaterials*, *35*(6), 1779–1788.

Wang, T. C., Rubner, M. F., & Cohen, R. E. (2002). Polyelectrolyte multilayer nanoreactors for preparing silver nanoparticle composites: Controlling metal concentration and nanoparticle size. *Langmuir*, *18*(8), 3370–3375.

Yamamoto, M., Kashiwagi, Y., & Nakamoto, M. (2006). Size-controlled synthesis of monodispersed silver nanoparticles capped by long-chain alkyl carboxylates from silver carboxylate and tertiary amine. *Langmuir*, *22*(20), 8581–8586.